Collisions between pulses of traveling-wave convection

Paul Kolodner
AT&T Bell Laboratories, Murray Hill, New Jersey 07974-0636
(Received 21 June 1991)

The first nonlinear state of traveling-wave convection in binary fluids with moderate negative separation ratio in a narrow geometry consists of "pulses": localized patches of convection whose spatial shape is fixed, and that drift at a velocity that depends on the local Rayleigh number. I present the results of two kinds of experiments on traveling-wave pulses. First, I study the behavior of pulses as they drift past narrow, fixed peaks in Rayleigh number. The pulses are sensitive to the Rayleigh number in a spatial domain that extends far ahead of the main body of the pulse. Second, I study collisions between pairs of counterpropagating pulses as a function of the velocity with which they approach one another. At high approach velocity, only one pulse survives the collision. At low approach velocity, a persistent double-peaked structure is formed. Under certain circumstances, this structure can be interpreted as a weakly bound state of two pulses.

PACS number(s): 47.25.Qv, 47.20.Ky

I. INTRODUCTION

In recent years, a great deal of experimental and theoretical effort has been directed at the problem of convection in a thin, horizontal layer of a binary fluid which is heated from below. The initial stimulus for the resurgence of interest in this classical problem came from the observation that, for a wide class of binary fluids, convection takes the form of *traveling waves* (TW's) [1]. Further experimental work revealed a fascinating feature of traveling-wave convection: the tendency, even in a narrow, quasi-one-dimensional geometry, to form confined states—that is, spatially restricted convecting regions which coexist stably with nonconvecting regions in a uniformly heated experimental cell [2–9]. A number of different steady [2–7] and dynamical [8,9] confined states of TW convection have been documented in recent experiments.

In this paper, I present the results of experiments on one particular type of confined state of TW convection: TW pulses. Pulses are confined states with a fixed spatial structure which are the first nonlinear TW state observed in a narrow experimental geometry for separation ratios Ψ in the range $-0.12 \lesssim \Psi \lesssim -0.07$ [4–7]. Pulses exhibit two important experimental properties. First, their amplitude profile bears a strong resemblance to a solitonlike solution of the lowest-order subcritical complex Ginzburg-Landau equation (CGLE) [4,10–12]. Second, in a cell of sufficient uniformity, pulses are observed to slowly drift in a direction parallel to that of the underlying TW, with a velocity that exhibits a shifted square-root dependence on the local stress parameter $\epsilon(x)$ [7].

The fact that the shape of experimental pulses resembles a solution of a CGLE raises the hope that the wealth of theoretical understanding of solitons and the CGLE that has been developed over the past two decades can be applied to explaining pulse dynamics as well. While the CGLE is used to model many nonequilibrium pattern-forming systems [12], it is especially attractive in the case of binary-fluid convection because the coefficients of all of its linear terms and some of its nonlinear terms can be calculated using a perturbation analysis of the full Navier-Stokes equations which describe convective motions in the Boussinesq approximation [13]. Substantial theoretical [13,14] and experimental [15,16] work has established a quantitative connection between this model equation and the actual physical system, at least in the linear and weakly nonlinear regimes.

However, TW pulses are not weakly nonlinear structures. Recent numerical integrations of the full Navier-Stokes equations have shown that the mechanism of confinement in this state is a large-scale concentration circulation which is manifestly not an infinitesimal perturbation of the diffusive, nonconvecting state seen below the onset of convection [17]. Thus a quantitative accounting of the dynamical behavior of TW pulses may also require the full Navier-Stokes equations and may not be possible using a model-equation approach. Nonetheless, the similarity between experimental pulse shapes and solutions of the CGLE suggests that a phenomenological CGLE model may be useful in this regard, even if a quantitative understanding is not to be expected. The object of the work described in this paper and in Ref. [7] is to present well-characterized experimental results which can test such a phenomenological CGLE model.

The second important feature of pulses—the dependence of their drift velocity on the local stress parameter—has an important practical application: it offers a convenient and accurate method for measuring and correcting accidental nonuniformities in the experimental convection cell. Thus, continuing the development of the diagnostic and calibration methods described in Ref. [7], I have installed an array of adjustable point heat sources on the underside of my convection cell and used pulse-drift information to correct thermal inhomogeneities to the level of a part in 10^4. I believe that this is now by far the most stable and uniform system available for the experimental study of pattern formation in one dimension.

The ability to create TW pulses, vary their drift velocity and control the local stress parameter $\epsilon(x)$ has made it possible to perform two kinds of experiments on the dynamical behavior of pulses. First, I study the drift of pulses past shaped profiles of $\epsilon(x)$. I have examined the effect of single, narrow peaks in $\epsilon(x)$, double peaks of various separations, and of broad, smooth features. Such experiments could be easily recreated using a model-equation approach. Second, I have produced pairs of counterpropagating pulses in a uniform $\epsilon(x)$ profile, set their velocity to a desired value, and observed their collision. Such collisions have already been the subject of numerical experiments based on coupled subcritical CGLE's with nonlinear-gradient terms [18].

The rest of this paper is organized as follows. Section II gives a brief description of the experimental apparatus and techniques. Section III describes the adjustments used to remove thermal inhomogeneities from the experimental cell. Section IV briefly describes experiments on the interaction of drifting pulses with spatial nonuniformities created by local heating in an otherwise uniform cell. Section V concerns collisions between pairs of counterpropagating pulses, and Section VI is a discussion.

II. APPARATUS

The apparatus used in these experiments has been described in great detail in Ref. [7], and so the discussion presented here will be brief. The cell consists of an annular channel of height $d=0.258$ cm, radial width $1.876d$, and mean circumference $92.0d$ (cell C in Ref. [7]). This channel is defined by a plastic disk and ring which are clamped between an electrically heated, mirror-polished silicon bottom plate and a water-cooled, polished sapphire top plate. The cell assembly is surrounded by foam insulation and sits on a vibration-isolated, level table. The geometrical uniformity of the cell has been carefully assessed: the radial width exhibits a fractional variation with azimuthal angle of better than 7×10^{-4}, and the fractional height variation is better than 3×10^{-4}. The typical temperature difference applied across the cell during these experiments is 6.1 °C and exhibits variations of typically 1.5×10^{-4} °C on short and long time scales. Thus the cell as constructed exhibits a Rayleigh number which is stable to 3 parts in 10^5 in time and to which geometrical nonuniformities contribute variations of about one part per thousand in space.

In order to compensate for spatial nonuniformities in the Rayleigh number, a set of twenty-four $\frac{1}{8}$-W, 100-Ω resistors has been pressed up against the underside of the silicon bottom plate of the cell, arrayed in a circle just outside the edge of the 9.55-cm-diam thin-film heater which provides the main heat flux in the experiment. The 24 "trim" resistors are wired in parallel with the main heater; each is connected in series with a variable adjustment resistor. Thus trim heating with an adjustable azimuthal profile and an amplitude proportional to the main heater output can be applied across the cell. Importantly, the spacing between adjacent trim resistors is 0.86 times the bottom-plate thickness, which in turn is 5.9 times the cell height. Thus the component of heat flux at the azimuthal spatial frequency of the trim-resistor spacing is reduced at the top surface of the silicon by a factor $\exp(2\pi/0.86)\sim1500$ by thermal diffusion. Since the total heat flux added by the trim heating is only about 1% of that of the main heater, the "washboard potential" caused by the spatially periodic trim heating is undoubtedly of negligible importance to the convection.

The main diagnostic used in these experiments is flow visualization by shadowgraphy. An afocal optical system projects white light onto the cell from above, and a reduced image of the reflection from the bottom plate is directed onto a circular camera, which consists of an annular array of 720 photodiodes. A small computer scans the camera at regular time intervals, displays the shadowgraph image intensity in real time, and stores the data for later analysis. As described in Ref. [7], this optical system exhibits such a low level of distortions that it can be used to measure lengths, and thus pulse velocities, with a precision exceeding 1%. The most useful processing performed on pulse data consists of computation of the pulse amplitude profile using spatial demodulation at the measured mean wave number. The position of the pulse is measured by computing the first moment of the amplitude profile, and this is differentiated in time to obtain the drift velocity. Velocities are scaled by κ/d, where d is the cell height and κ is the thermal diffusivity of the fluid. In cases where counterpropagating pulses are studied, the two amplitude components are first separated using full complex demodulation [19]. Their positions can then be followed separately. These techniques have been described in great detail in Refs. [7] and [19]. The fluid used in these experiments is 2.8 wt % solution of ethanol in water at a mean temperature of 28.2 °C. This fluid has separation ratio $\Psi=-0.123$, Prandtl number $P=7.00$, and Lewis number $L=0.0088$ [20].

III. DRIFTING PULSES AND THE QUEST FOR THE PERFECT CONVECTION CELL

The experiments described in this paper begin with the determination of the temperature difference applied across the cell ΔT_{co}, which corresponds to the onset of convection. As described in Ref. [7], this measurement consists of servoing the applied temperature difference ΔT so that linear TW's exhibit a vanishing temporal growth rate. The stress parameter ϵ associated with other values of ΔT is defined with respect to this threshold: $\epsilon\equiv(\Delta T-\Delta T_{co})/\Delta T_{co}$. In a nonuniform cell, ϵ may be a function of spatial position x; in this case, the fractional amount by which ΔT exceeds ΔT_{co} corresponds to the spatial average of $\epsilon(x)$ and is denoted $\bar{\epsilon}$.

With the onset of convection thus determined, TW pulses can be produced using techniques described in Ref. [7]. The physical phenomenon that is the basis for the results reported in this paper is illustrated in Fig. 1, which shows the drift velocity v_{dr} of noninteracting TW pulses as a function of ϵ. Figure 1 corresponds exactly to the data reported in Fig. 15 of Ref. [7]; however, the refinements in cell uniformity described in this section have led to such an improvement in the precision of the

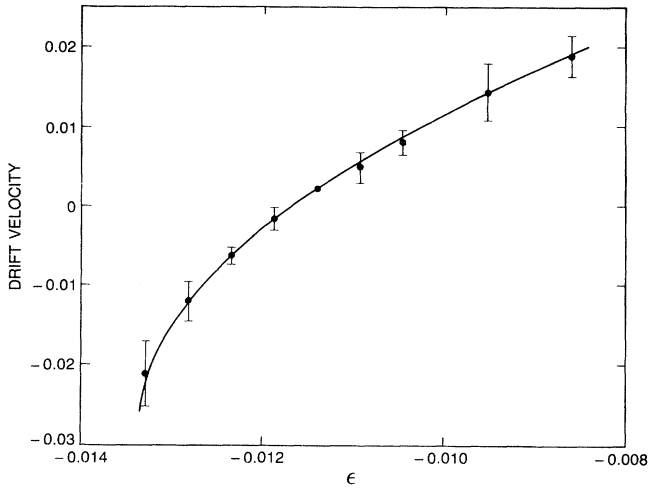

FIG. 1. The drift velocity of isolated TW pulses is plotted as a function of the stress parameter ϵ. The data points are measurements, and the smooth curve has the form $v_{dr}(\epsilon)=-v_0+a(\epsilon+\epsilon_0)^{1/2}$. The least-squares-fit parameters found for these data are $v_0=0.028$, $a=0.682$, and $\epsilon_0=0.0133$. Note that the error bars have been magnified by a factor of 5 for clarity.

data that the error bars in Fig. 1 have had to be magnified by a factor of 5 for visibility [21]. Typically, v_{dr} can be measured at a particular value of ϵ with an uncertainty of ± 0.0002 to ± 0.0013. This level of precision has been crucial in experiments on interacting pulses, as described below.

As shown by the smooth curve in Fig. 1, the dependence of v_{dr} on ϵ can be inverted using a parabolic fit to $\epsilon(v_{dr})$. Thus local measurements of $v_{dr}(x)$ can be used to map the spatial variation of $\epsilon(x)$, and this procedure was discussed in some detail in Ref. [7]. Figure 2 illustrates how this stress-parameter diagnostic can be used to correct nonuniformities in $\epsilon(x)$. Figure 2(a) shows the spatial dependence of the pulse drift velocity $v_i(x)$ measured with no power applied to the trim resistors. As shown by the calibration on the right-hand axis of Fig. 2(a), the broad dip in $v_i(x)$ centered near location 270° in the cell corresponds to a peak-to-peak variation of about 0.005 in the stress-parameter profile $\epsilon_i(x)$. In light of the estimate above that geometrical nonuniformities in the cell can only account for a variation in $\epsilon(x)$ of about 0.001, it seems likely that nonuniform heating of the bottom plate of the cell is its dominant cause. Thus compensation by adjustable local heating seems quite a reasonable cure.

I denote the change in the stress-parameter profile caused by applying a unit electrical power to the jth trim resistor at location x_j by $\Delta\epsilon(x-x_j)$. This function exhibits a peak at $x-x_j=0$ which has a spatial width comparable to the thickness of the bottom plate of the cell. With this, the total change in $\epsilon_i(x)$ caused by energizing the entire resistor array is

$$\epsilon_h(x)=\sum_j h_j\Delta\epsilon(x-x_j)\ , \tag{1}$$

where h_j is the power applied to the jth resistor. Compensating the nonuniformities in $\epsilon_i(x)$ requires adjusting the h_j so that $\epsilon_i(x)+\epsilon_h(x)$ exhibits as small a spatial variation as possible. This problem is solved in two steps. First, the function $\Delta\epsilon(x-x_j)$ must be calculated. For the present purposes, I have found it entirely satisfactory merely to compute the temperature profile in the plane of the top of the silicon plate that would be due to a point source of heat in an infinite conducting medium:

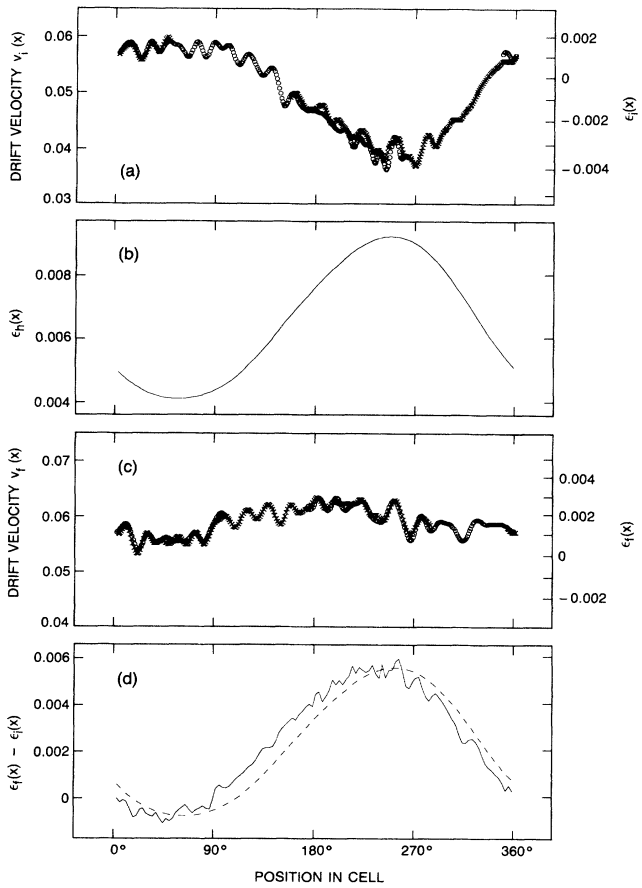

FIG. 2. (a) Drift velocity profile measured for a state of two right-going pulses (symbols × and ○) at $\bar{\epsilon}=-0.0006$ with no trim heating. The stress-parameter profile $\epsilon_i(x)$, which is calibrated along the right-hand axis, exhibits a dip near location 270°. (b) The increase $\epsilon_h(x)$ calculated using Eq. (1), using coefficients based on the profile $\epsilon_i(x)$ in (a). This trim heating produces a local peak in $\epsilon(x)$ near location 270° to match the dip in (a). (c) Drift velocity profile measured at $\bar{\epsilon}=0.0018$ with trim heating corresponding to the profile $\epsilon_h(x)$ in (b). The nonuniformity in the stress-parameter profile is much reduced from that in (a). (d) Full curve: difference $\epsilon_h(x)-\epsilon_i(x)$ between the stress parameters profiles measured (c) with and (a) without the trim heating. This difference profile measures the pulse response to the trim heating profile in (b), which is reproduced as the dashed curve. The response is shifted laterally because the pulse responds to the stress parameter ahead of its center. A shift in the opposite direction would be obtained from measurements using left-going pulses.

$\Delta\epsilon(x-x_j)=\alpha/|\mathbf{x}-\mathbf{x}_j|$. Here the vector notation in the denominator is used to indicate that the relevant distance is the length of the vector connecting the local of the resistor on the bottom surface of the silicon plate and the location x on the top surface; the constant α has been estimated from the thermal properties of silicon. The second half of the problem consists of computing the constants h_j, and this, unfortunately, constitutes an inverse problem without an analytical solution. However, the following solution is adequate. I start by smoothing the measured profile $\epsilon_i(x)$, shifting a distance δ (δ is initially set at 4.4 times the cell height d, a somewhat imprecise result obtained in Ref. [7]), and setting

$$h_j=\beta[\epsilon_{\max}-\epsilon_i(x_j-\delta)] . \tag{2}$$

Here $\epsilon_{\max}$ is the maximum value in the profile $\epsilon_i(x)$, and β is another thermal constant which can be estimated. Figure 2(b) shows the function in Eq. (1) computed using these values for h_j. Aside from the small-scale wiggles in the measured drift velocity $v_i(x)$, it is clear that adding this profile to that in Fig. 2(a) will improve the uniformity of the stress parameter. And, as shown in Fig. 2(c), this is indeed the case. The profile $\epsilon_f(x)$ measured with the resistor array energized according to the prescription of Eq. (2) is already improved by a factor of 4.

The spatial shift δ has so far been set to $4.4d$, and the product $\alpha\beta$ has only been roughly estimated. The velocity profiles shown in Figs. 2(a) and 2(c) can be used to determine both of these parameters quite precisely. The full curve in Fig. 2(d) shows the measured difference $\delta\epsilon(x)\equiv\epsilon_f(x)-\epsilon_i(x)$ computed from those profiles. $\delta\epsilon(x)$ is the response of the pulse to the additional heating $\epsilon_h(x)$ from the trim resistors—this is reproduced as the dashed curve in Fig. 2(d). Not surprisingly, $\delta\epsilon$ is found to be linearly related to a laterally shifted version of ϵ_h: $\delta\epsilon(x)=a+b\epsilon_h(x-\delta')$. The parameters a and b are determined using a simple least-squares linear fit, and δ' is varied until the rms error of this fit is minimized. Because of the details of how the bottom-plate temperature is controlled in the apparatus, the offset a has no meaning. The parameter b is the factor by which the initial estimate of the product $\alpha\beta$ was in error, and δ' is the true spatial shift. I find that the correct spatial shift is $\delta'=3.8$ times the cell height. In comparing this result with the initial estimate of $4.4d$, it should be recalled that the previous result came from experiments in a different fluid in which the profile corresponding to $\epsilon_i(x)$ was compared with the profile deduced from measurements of the state of linear TW's seen at onset. The present result is a much more direct and reliable one. Also, the profiles in Fig. 2(d) show the response of the pulse velocity to a broad feature in $\epsilon_h(x)$. Experiments on the drift of pulses past sharp peaks in $\epsilon_h(x)$ are described in Sec. IV.

The velocity profile shown in Fig. 2(c) is in fact the end result of the iterative procedure just described, and a peak-to-peak nonuniformity of about 0.0015 is still evident. The compensation is imperfect because the prescription in Eq. (2) is only an approximate solution to the inverse problem. However, now that the parameters $\alpha\beta$ and δ are accurately known, the $\epsilon(x)$ profile corresponding to an arbitrary set of heater powers h_j can be calculated easily using a short computer program, and it is not too time consuming to improve the compensation obtained above by adjusting the h_j by hand. This procedure could also be performed using an optimization routine. With some experience, the adjustment can be done so well by hand that a rms variation of as little as 2×10^{-5} in the computed $\epsilon_f(x)$ profile is obtained. With the series resistances in the apparatus adjusted according to this optimized prescription, a substantially improved experimental homogeneity is obtained. Figure 3 shows a typical example. In this case, the variation in $\epsilon(x)$ consists dominantly of high-spatial-frequency wiggles; there is practically no nonuniformity at low spatial frequency. I do not know the true cause of the wiggles in this velocity profile. The results of Sec. IV, in which it is shown that the pulse velocity has an attenuated response to sharp features in $\epsilon(x)$, suggests that real nonuniformities in the cell are not the cause. Part of this high-spatial-frequency component is reproducible from run to run and is likely to be the result of residual distortions in the optical system. However, the pulse shape also tends to exhibit small asymmetries and modulations [6,7], and these affect the first moment of its amplitude profile and hence the velocity measurement. My estimate is that most but not all of this high-spatial-frequency component is an artifact. The rms variation of $\epsilon(x)$ for the run in Fig. 3 was 3.4×10^{-4}; filtering out the wiggles by convoluting $\epsilon(x)$ with the measured pulse amplitude profile [7] reduced this by a factor of 3. My best attempt at compensating nonuniformities exhibited a rms variation in $\epsilon(x)$ of 6×10^{-5} after lopass filtering. The long-term stability of these results is the subject of ongoing measurement; however, my experience so far is that the rms spatial variations in $\epsilon(x)$ do not grow worse than 2 to 4×10^{-4} in the course of a week or two. For all but the most sensitive experiments on low-velocity pulse collisions, the nonuniformity of this cell is unimportant and remains so.

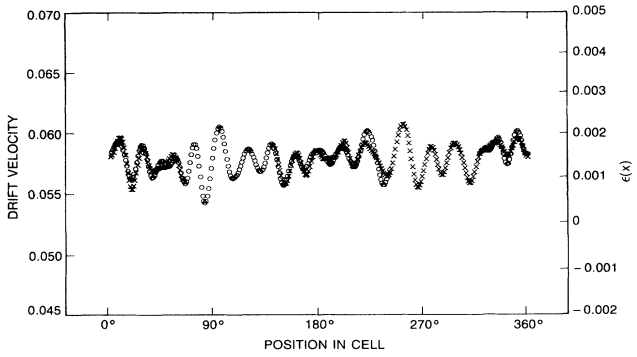

FIG. 3. Drift velocity profile measured for a state of two pulses at $\bar{\epsilon}=0.0016$ after further hand optimization of the trim resistor powers. This cell exhibits nonuniformities of 1–3 parts in 10^4, depending on whether the high-spatial-frequency components are included. This extreme uniformity can be maintained for weeks, and it can be further improved.

IV. INTERACTIONS OF PULSES WITH LOCALIZED NONUNIFORMITIES IN RAYLEIGH NUMBER

The techniques described in the preceding section make it easy to study the response of pulses to shaped profiles of $\epsilon(x)$. The simplest such experiment that can be performed consists of changing the heating power dissipated by a single one of the trim resistors, and then measuring the velocity of pulses which drift past the resulting narrow feature in $\epsilon(x)$. Figure 4 shows the result of two such experiments. The dashed curve in Fig. 4(a) shows the $\epsilon(x)$ profile imposed on the system by increasing the heat dissipated in one trim resistor. This profile was calculated assuming, as in the preceding section, that the temperature field in the silicon bottom plate is simply proportional to the inverse of the distance between the source and the measurement point. Clearly, this approximation neglects the effects on the temperature field of the insulating boundaries at the edge of the apparatus and of the different thermal conductivities of the materials of which the cell is constructed. Including these effects in an analytical or numerical calculation of the temperature field would be straightforward. However, because of the limited reproducibility of the results in the section, I do not think that such an effort would be justified.

The response of two left-going pulses which drift through the peak in $\epsilon(x)$ is shown by the full curve in Fig. 4(a). This profile was computed by measuring the drift-velocity profile $v_{dr}(x)$ and using the curve in Fig. 1 as a calibration. The dominant feature of the pulse response $\epsilon(v_{dr}(x))$ is that the drift-velocity profile is noticeably broader than the imposed stress-parameter profile $\epsilon(x)$. This is also clear in Fig. 4(b), which shows the result of one of several experiments in which pulses drifted past pairs of peaks in $\epsilon(x)$ at various spacings. Consistent with the broadening seen in Fig. 4(a), the depth of the valley between the two peaks in $\epsilon(x)$ is substantially reduced in the pulse response $\epsilon(v_{dr}(x))$.

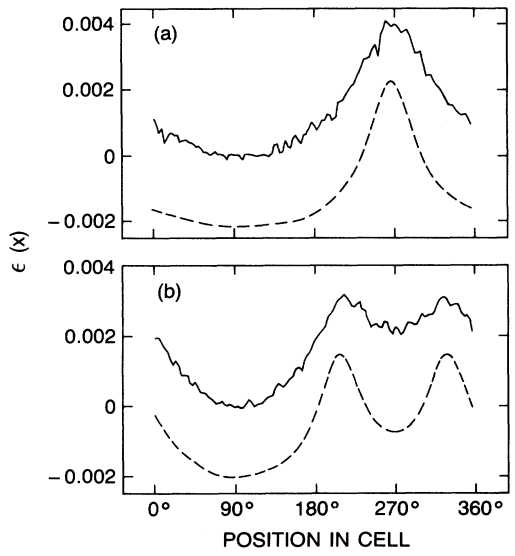

FIG. 4. Results of two experiments in which left-going pulses were allowed to drift past sharp features in $\epsilon(x)$. The dashed curve in (a) shows the input $\epsilon(x)$ profile computed for a run in which excess power was dissipated in one of the trim-heating resistors underneath the cell. The full curve shows the pulse response $\epsilon(v_{dr}(x))$ computed from the drift-velocity profile $v_{dr}(x)$, using the calibration in Fig. 1. (b) shows the result of applying excess heat at two points separated by $31d$. The pulse responds to a spatially lopass-filtered version of $\epsilon(x)$, resulting in a broadening of the single peak in (a) and a filling-in of the dip between the two peaks in (b). The dashed curves have been displaced vertically for clarity.

I have characterized the response of pulses to features imposed in $\epsilon(x)$ by assuming that the measured response profile $\epsilon(v_{dr}(x))$ is equal to the convolution of the applied profile $\epsilon(x)$ with a kernel function $k(x)$. The kernel has been computed for each of seven runs by dividing the Fourier transforms of $\epsilon(v_{dr}(x))$ and $\epsilon(x)$, removing the high-frequency part of the ratio with an adjustable filter, and performing an inverse transform. The high-frequency filter has several parameters, and an optimization algorithm is used to adjust them so that the rms difference between $\epsilon(v_{dr}(x))$ and the explicitly calculated convolution of $\epsilon(x)$ with $k(x)$ is minimized. Figure 5 shows that this procedure works very well. There, the full curve shows the response $\epsilon(v_{dr}(x))$ for the run in Fig. 4(b), and the dashed curve shows the convolution of the applied $\epsilon(x)$ profile with the computed kernel.

The full curve in Fig. 6(a) shows the convolution kernel computed for a run in which right-going pulses drifted past a double peak in $\epsilon(x)$. For comparison, the dashed curve shows the amplitude profile of a right-going pulse measured at $\epsilon = -0.0084$ [7]. The kernel consists of a narrow central peak and several sidelobes. The centroid of the kernel is displayed noticeably ahead of that of the pulse. The run-to-run reproducibility of the details of the

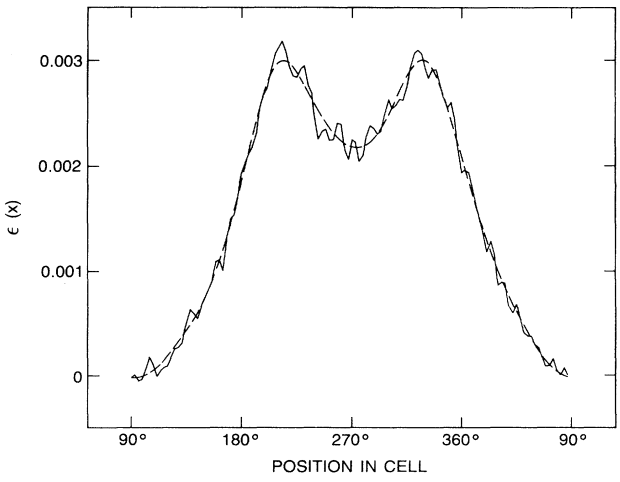

FIG. 5. The full curve repeats the response profile $\epsilon(v_{dr}(x))$ in Fig. 4(b). The smooth, dashed curve shows the convolution of the applied $\epsilon(x)$ profile [dashed curve in Fig. 4(b)] with the kernel computed by the deconvolution algorithm. The horizontal axis has been shifted for clarity.

shape of the convolution kernel—for example, of the spacing and height of the sidelobes—is only fair. What is striking and reproducible is that the sidelobes contribute substantial weight far ahead of the centroid of the pulse. One measure in which this is apparent is the width of the kernel, as parametrized by its second moment. In Ref. [7], I defined the second-moment length L_2 as the square root of the ratio of the second and zeroth moments. The computed kernels exhibit L_2 values in the range $4.3d-5.4d$, while $L_2=1.9d$ for a pulse at the measured spatially averaged stress parameter $\bar{\epsilon}=-0.005$ [7]. I cannot discern systematic differences between kernels measured with single peaks in $\epsilon(x)$ and those measured with double peaks (the spacing between peaks was varied from $22d$ to $35d$).

Figure 6(b) shows the kernel which represents the pulse response to broad features in $\epsilon(x)$. This kernel was computed using the two curves in Fig. 2(d), and its shape is strikingly different from the kernel obtained from experiments on sharp features in $\epsilon(x)$. Here, a very broad, double-humped shape is obtained. The first moment $3.8d$ matches the value of the shift δ' obtained in Sec. III, as it must. While the main body of this kernel is much broader than that of the kernels obtained with narrow peaks in $\epsilon(x)$, the lack of far sidelobes causes its second moment to be somewhat smaller: $L_2=3.6d$. But the main feature seen in the preceding paragraph still obtains: the pulse is strongly sensitive to the conditions far ahead of its centroid.

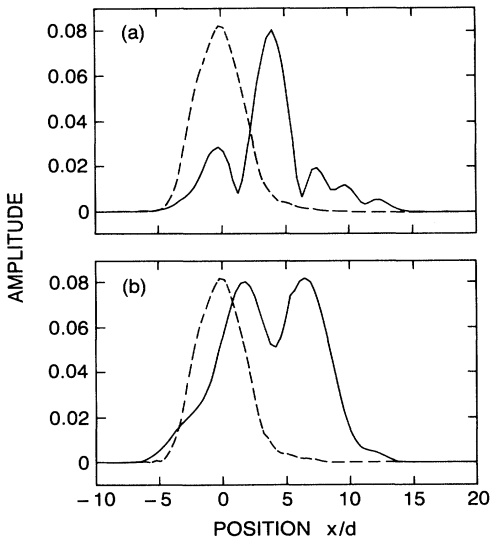

FIG. 6. (a) The full curve shows the convolution kernel computed for a run in which right-going pulses drifted past a pair of peaks in $\epsilon(x)$ separated by $22d$. For comparison, the dashed curve shows the amplitude profile of a right-going pulse measured at $\epsilon=-0.0084$, taken from Fig. 16 of Ref. [7]. The kernel is shifted to the leading edge of the pulse and has substantial weight at distances far ahead of the centroid of the pulse. (b) Full curve: kernel computed from the drift of right-going pulses past the broad $\epsilon(x)$ profile in Fig. 2(d). The kernel exhibits a striking broad, double-humped shape. Again, much of the weight of the kernel is found at distances far ahead of the centroid of the pulse.

V. COLLISIONS BETWEEN PULSES

The ability to set the drift velocity of TW pulses by adjusting $\bar{\epsilon}$ now offers the opportunity to study controlled collisions of pairs of counterpropagating pulses. Several such experiments have been conducted, under conditions of good to excellent uniformity of $\epsilon(x)$. The nature of the collisions seems to depend only on the velocity with which the pulses approach each other. As a consequence, I quote the drift velocity as the principal independent variable in this section, rather than $\bar{\epsilon}$. In addition to appearing physically reasonable, this choice has the experimental advantage of being directly and quickly measurable before and after pulse collisions (the experimental control parameter $\bar{\epsilon}$ for specific runs will be quoted in the figure captions). However, since interacting pulses are observed to accelerate, decelerate, and even coexist without moving, it is necessary to be precise: In this section, the term "drift velocity" is reserved to indicate only the "bare" drift velocity each pulse would have under the conditions of the experiment in the absence of the other pulse. The propagation of interacting pulses, which may move at a velocity different from the bare drift velocity, will be characterized by other terms, such as "approach velocity" or "separation velocity."

Another point of nomenclature is in order. This section describes interactions between pairs of adjacent *counterpropagating* pulses, that is, the vector *phase* velocities of the underlying TW point in opposite directions. If the phase velocity vectors of the two pulses point towards the space in between the two pulses, they are referred to as *forward facing*. Absent interactions, forward-facing pulses would move apart at negative drift velocity and would move together at positive drift velocity. The opposite situation, in which the phase velocity vectors of two adjacent pulses point away from the space in between them, is referred to with the term *backward facing*. Backward-facing pulses move apart at high enough positive drift velocity.

As a final point of clarification, the reader should note that the quantitative results presented in this section were obtained in experiments on *fully developed* pulses, which interacted over periods of many hours. Thus these results pertain to pulses whose amplitude profiles in isolation are well described by the results in Fig. 17 of Ref. [7]. I have not felt that experiments on interactions between pulses in different stages of evolution could be controlled well enough to merit quantitative attention. The reader may note that some of the runs presented in this paper began with pulses that had not quite equilibrated. For example, a difference in the initial pulse shapes is noticeable in Fig. 9. Since the time scale of the evolution of the pulse amplitude profile is about an hour, the interaction in even this run was between fully developed pulses. More importantly, the qualitative features of the interaction in the run of Fig. 9 (as well as in the pulse interac-

tions illustrated in Figs. 7 and 13) are not different from those seen in other runs which began with fully developed pulses.

Figure 7 illustrates the interaction between two forward-facing pulses which approach at a moderately high, positive velocity. As shown in the *hidden-line plot* in Fig. 7(a), the pulses drift together and experience a catastrophic interaction whose result is a single pulse of right-going TW which drifts off to the right. The *phase plot* in Fig. 7(b) shows the nature of the interaction in greater detail: after the pulses come together, the left-going pulse shrinks away and vanishes. This leaves a broad packet of rapidly propagating right-going TW [note the increased phase velocity at times 17 000–22 000 sec in Fig. 7(b)], which gradually evolves back into a normal right-going pulse. A destructive interaction of this type is always the result of a collision at high approach velocity; a similar collision was reported in Fig. 5 of Ref. [7], for a fluid with $\Psi=-0.072$. In Ref. [6], Fig. 15, a somewhat similar interaction between adjacent counterpropagating pulses was observed, using a fluid with $\Psi=-0.069$. There, we observed that the interaction was accompanied by the emission of a burst of linear TW's. In the present case, it is not possible to say whether the same emission takes place. For the present separation ratio, the low drift velocities required for controlled pulse-collision experiments are achieved so far below the onset of convection that linear TW's disappear too quickly to be observed.

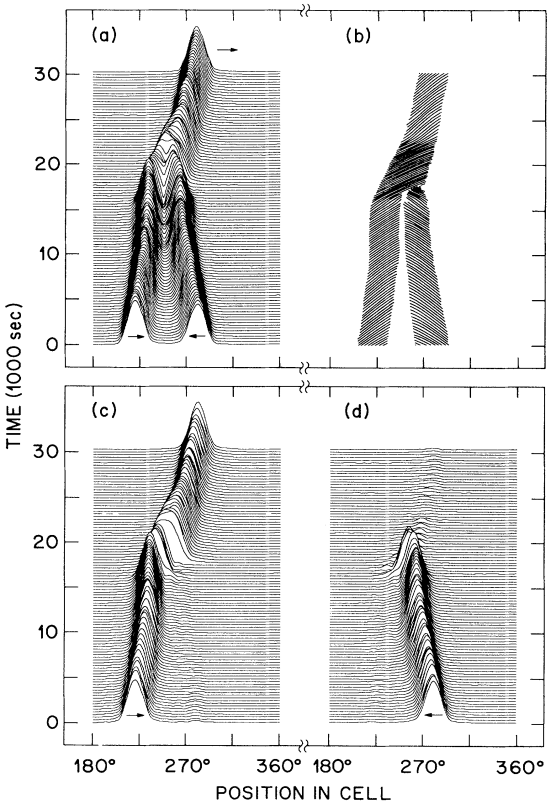

FIG. 7. Destructive collision between two counterpropagating TW pulses at $\bar{\epsilon}=-0.0088$. (a) Profiles of the total demodulated wave amplitude computed at successive instants in time are displaced vertically to produce a hidden-line plot. As indicated by the horizontal arrows underneath the lowest profile, these pulses drift together at positive velocity, i.e., parallel to the direction of the underlying TW. (b) Lines of constant TW phase are plotted in space-time to produce a phase plot of the interaction in (a). The interaction of the pulses causes the left-going component to shrink and disappear over the course of about 2000 sec. This leaves a broad pulse of rapidly propagating TW, which evolves back into a normal, right-going TW pulse. (c) Right-going component of the interaction in (a), extracted using complex demodulation. (d) Left-going component.

Figures 7(b) and 7(c) show the left- and right-going TW components during the interaction, computed using complex demodulation. Using these separated peak profiles, it is possible to plot the path of each of the pulses in space-time during their interaction. This is shown in Fig. 8. Initially, the two pulses drift together with velocity 0.0014 ± 0.0002. At $t=17\,400$ sec in Fig. 8, which corresponds to the beginning of the plots in Fig. 7, the Rayleigh number is increased, and the pulses begin to move together with an average approach velocity of about 0.02. The space-time plot reveals quite clearly that the pulses begin to decelerate when their centroids approach within about $10d$ of each other, leading to a brief period

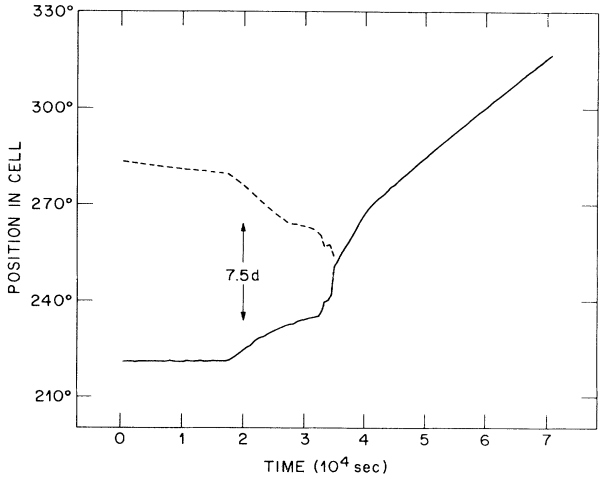

FIG. 8. The space-time paths of the centroids of the right-going (full curve) and left-going (dashed curve) pulses during the interaction in Fig. 7. The vertical arrow of length $7.5d$ has been included as a distance reference. Initially, the pulses drift together at velocity 0.0014 ± 0.0002 ($\bar{\epsilon}=-0.0115$). The initial slight drift of the average of the two pulse positions seen here and in Fig. 14 below is caused by a very weak residual gradient in $\epsilon(x)$. At time $t=17\,400$ sec, corresponding to the beginning of the plots in Fig. 7, $\bar{\epsilon}$ is changed to -0.0088, causing an increase in the approach velocity to approximately 0.02. After a brief deceleration at separation $\sim 7.5d$, the pulses rush together and interact, leaving a right-going pulse which drifts away at velocity 0.0180 ± 0.0003.

($t=28\,000$–$33\,000$ sec) in which the distance between pulses is stuck at about $7.5d$. This is to be compared with the pulse width of about $4.6d$ full width at half maximum [7]. Then, at $t=34\,000$ sec, the separation between pulses rapidly collapses as the left-going pulse is destroyed. The subsequent drift of the remaining right-going pulse provides an accurate calibration of the drift velocity which characterizes the interaction: $v_{dr}=0.0180\pm0.0003$.

Annihilation of one of the pulses is not the only outcome of a collision between forward-facing pulses at positive drift velocity. Figure 9 shows a collision of two pulses which approach at $v_{dr}=0.0107\pm0.0006$. At this reduced drift velocity, the pulses simply come to a stop, forming a double-peaked structure which will persist indefinitely if the experimental parameters are left unchanged. The spacetime plot in Fig. 10 shows the rather abrupt deceleration of the pulses in this collision. The distance between pulse centroids in the two-pulse structure is 8.05 ± 0.02 times the cell height.

Once this double-peak structure has been created, it can be probed by varying the Rayleigh number or, equivalently, the drift velocity v_{dr} each pulse would have at that Rayleigh number in the absence of the other pulse. Figures 11(a) and 11(b) show the result of increasing and decreasing v_{dr}. In Fig. 11(a), the initial drift velocity is 0.0149 ± 0.0008, and the initial spacing between pulses is $7.905d\pm0.017d$. Increasing v_{dr} to 0.0176 ± 0.0010 causes the pulses to move closer together, and the final increase, to $v_{dr}=0.0195\pm0.0008$, precipitates a destructive interaction of the type in Fig. 7. In Fig. 11(b), initially separated pulses are brought together at $v_{dr}=0.0095\pm0.0007$. After the structure has stabilized, v_{dr} is gradually reduced, and the separation grows. With the final drop to $v_{dr}=-0.0003\pm0.0005$ at $t=137\,600$ sec in Fig. 11(b), the pulse separation increases without stabilizing.

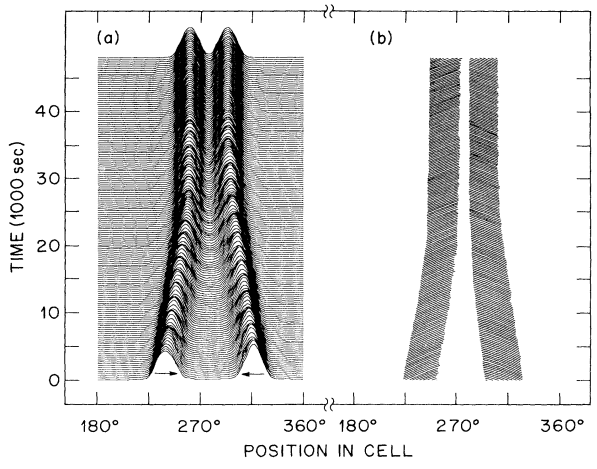

FIG. 9. Nondestructive collision between two counterpropagating pulses which approach each other at velocity 0.0107 ± 0.0006 ($\bar{\epsilon}=-0.0101$). (a) Hidden-line plot showing the demodulated pulse amplitude profiles. (b) Phase plot showing the propagation of the underlying TW.

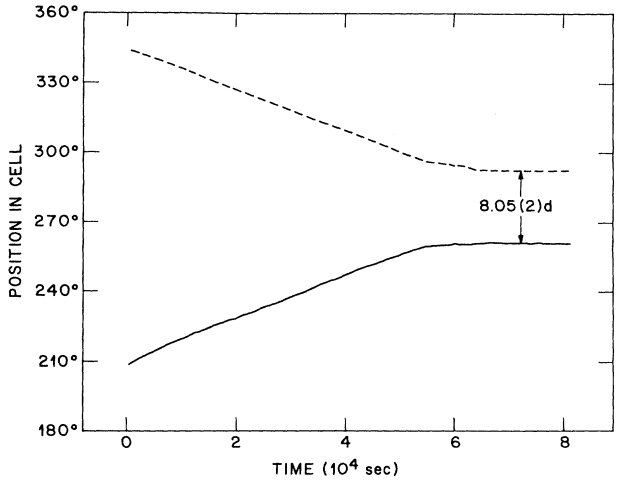

FIG. 10. Space-time paths of the pulse centroids during the interaction of Fig. 9. The pulses drift together at constant, positive velocity and then abruptly slow down and stop, at a separation of $8.05d\pm0.02d$. The beginning of the plots in Fig. 9 corresponds to $t=33\,000$ sec in this graph.

In Fig. 12, the results of several runs like the ones in Figs. 11(a) and 11(b) are brought together in a plot of pulse separation vs drift velocity. The pulse separation diverges at a drift velocity consistent with zero and drops monotonically with increasing drift velocity, forming something of a plateau at a separation of about $8d$. At a velocity of about 0.02, the pulse separation drops to zero as one pulse is destroyed. The fact that the pulses separate when their drift velocity is reduced below zero, combined with the absence of a minimum in the dependence of separation on drift velocity, implies that the double-pulse structures do not constitute true bound states. Rather, the pulses behave as if they are being pushed together against a mutual repulsion by a force proportional to the drift velocity. The repulsion is overcome if the pulses are pushed closer together than about $7.5d$; in this case, they interact catastrophically.

Because of the region of negative drift velocity in Fig. 1, it is possible to collide backward-facing as well as forward-facing pulses. Figures 13 and 14 show the results of a collision at $v_{dr}=-0.0104\pm0.0008$. The hidden-line plot of Fig. 13(a) shows that only one pulse survives in this case, as in Figs. 7 and 8. However, inspection of the phase plot in Fig. 13(b) shows that the destructive interaction in this case is qualitatively different than that seen for fast forward collisions. Instead of a gradual decay of one of the two pulses in favor of the other, the entire double-peaked structure loses stability abruptly, and a new, single pulse appears after a short delay. The suddenness of the destructive interaction is more apparent in hidden-line plots of the individual left- and right-going components [Figs. 13(c) and 13(d)]. At the instant of destruction, each component exhibits a pulse-shaped burst of amplitude at the location of

the oppositely-propagating pulse. These bursts are caused by transient leakage through the demodulator filters. This is numerical artifact, typically seen at the ends of data series, where the outputs of the digital filters have not yet settled. The appearance of such a transient at the moment of pulse destruction means that the event is accompanied by a 100% change in signal amplitude over the course of one or two time steps. This represents a time of less than one oscillation period. The sudden collapse of the two pulses is also seen in the space-time plot shown in Fig. 14. The pulses approach one another at essentially constant velocity until their spacing decreases to about $7.5d$. They then quickly collapse and form the output pulse.

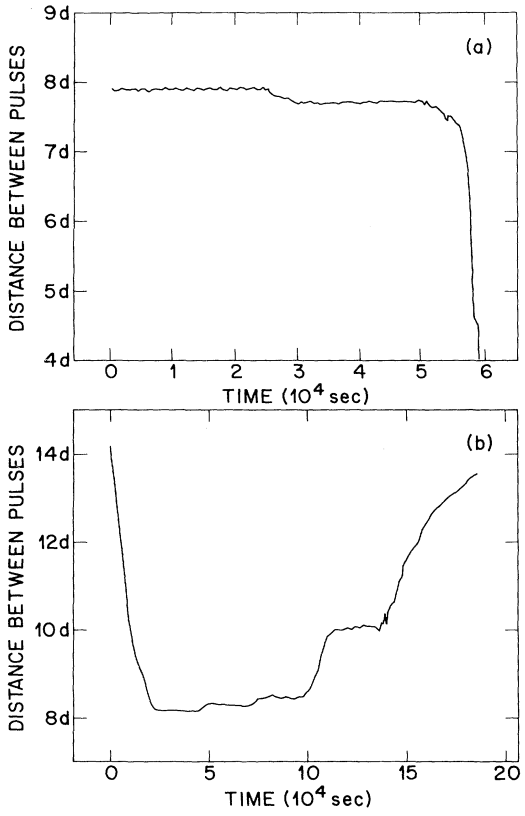

FIG. 11. (a) The distance between pulse centroids in the structure in Fig. 9 is plotted as a function of time as the approach velocity is slowly increased. Initially, $v_{dr}=0.0149\pm0.0008$. At $t=25\,200$ sec, the velocity is increased to $v_{dr}=0.0176\pm0.0010$, and the pulses move closer together. At $t=50\,400$ sec, the velocity is increased to $v_{dr}=0.0195\pm0.0008$, and the pulses collapse as in Fig. 7. (b) Distance between pulses vs time for another pulse pair. Initially, the pulses approach at $v_{dr}=0.0095\pm0.0007$. At $t=48\,100$ sec, the velocity is decreased to $v_{dr}=0.0069\pm0.0003$, and the pulse separation increases slightly and stabilizes. Subsequent decreases in v_{dr} to 0.0045 ± 0.0005 at $t=73\,300$ sec and to 0.0019 ± 0.0003 at $t=98\,500$ sec cause further increases in pulse separation. Following the final decrease to $v_{dr}=-0.0003\pm0.0005$ at $t=137\,600$ sec, the pulses drift apart.

As in the case of pulses which approach at positive velocity, backward-facing pulses which approach at a sufficiently small negative drift velocity can form a composite, double-pulse state whose amplitude profile is time independent. Subsequently making the drift velocity more negative again causes the pulses to move closer together and then to annihilate. Such an event is shown in Fig. 15. Remarkably, even though the run in Fig. 15 started with two motionless adjacent pulses, and even though the increase in the magnitude of the drift velocity was quite small the collapse of the double-pulse structure was just as abrupt in this case as in the run of Figs. 13 and 14.

Figure 16 shows the distance between pulse centroids in a state of two backward-facing pulses as a function of the drift velocity each would have if isolated. As in the case of forward-facing pulses, I find a monotonic dependence on drift velocity which exhibits a weak plateau at a separation of about $8d$. Now, however, the existence of persistent double-pulse states at positive drift velocity

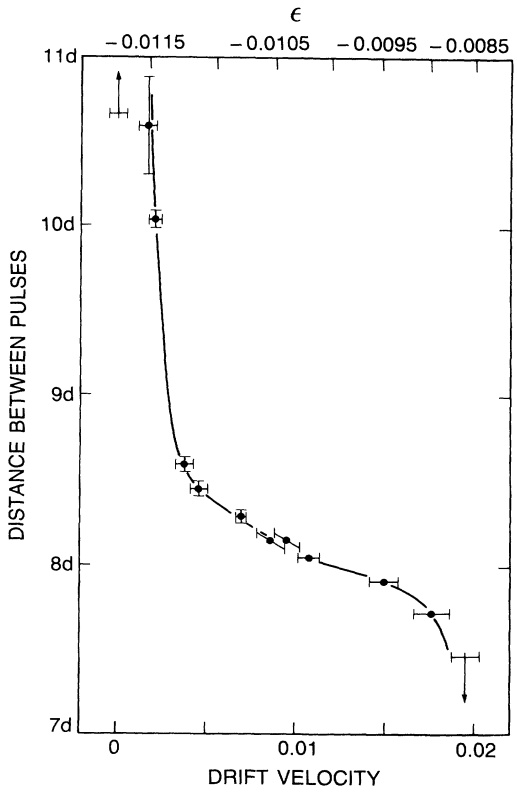

FIG. 12. The distance between pulse centroids measured in runs like those in Fig. 11 is plotted as a function of drift velocity. The scale along the top horizontal axis of the graph gives the value of ϵ which corresponds to the drift velocity on the bottom horizontal axis, as determined from the calibration in Fig. 1. As indicated by the vertical-arrow symbols, the pulses drift apart for $v_{dr}\sim0$ and collapse at $v_{dr}\sim0.02$. In between, the separation is a monotonically decreasing function of drift velocity. Several of the data points have vertical error bars which are too small to be displayed. The curve is a guide to the eye.

suggests that a *bound state* has been formed, in contrast to the previous case of forward-facing pulses, which moved apart when the drift velocity was decreased to zero.

However, the extremely small velocities and long time scales encountered in these experiments necessitate a more careful examination of the evidence for a bound state. Figure 17 shows the time history of the pulse separation during part of the run on which Fig. 16 is based. At time $t=0$ [indicated by the arrow marked (a)], the drift velocity was increased from -0.0027 ± 0.0006 to -0.0002 ± 0.0003. Following a transient, the pulse separation settled to 8.62 ± 0.03 times the cell height. Such

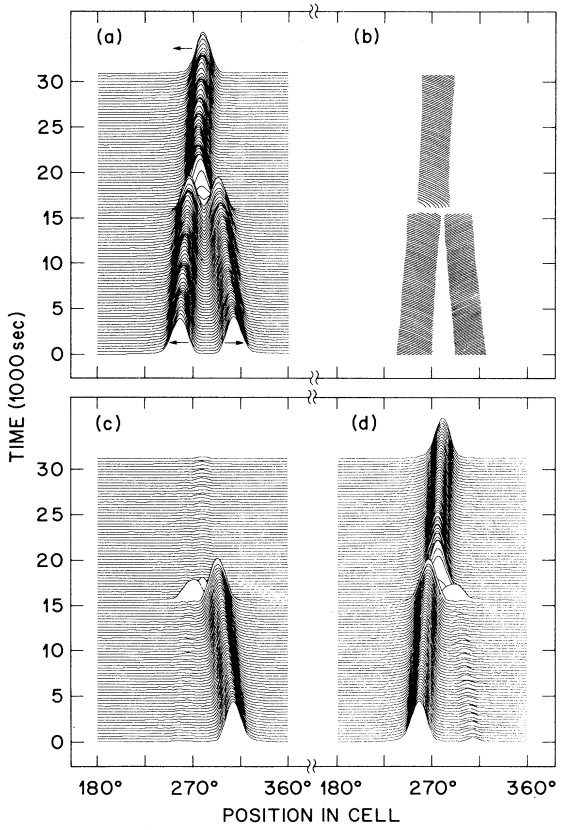

FIG. 13. Destructive interaction of two backward-propagating pulses at approach velocity -0.0104 ± 0.0008 ($\bar{\epsilon}=-0.0127$). (a) Hidden-line plot of total demodulated wave amplitude. (b) Phase plot showing the propagation of the individual TW. At time $t=15\,750$ sec, the composite double-pulse structure abruptly disappears, to be replaced by a left-going pulse. (c) Right-going component of the TW in (a). (d) Left-going component. The transient appearance in the plot of each separate amplitude of a pulse at the location of the other is a numerical artifact which indicates that the destruction of the pulses occurred in a time as short as only one or two time steps, which is comparable to one oscillation cycle.

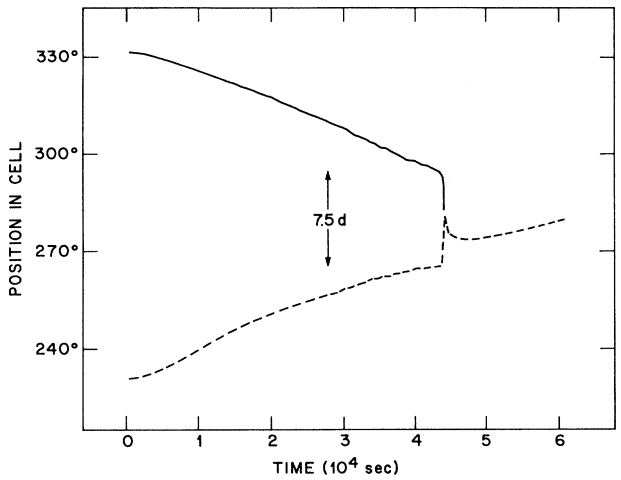

FIG. 14. The paths of the two interacting pulses in Fig. 13 are plotted in space-time. Because of a very slight nonuniformity in $\epsilon(x)$, the incoming pulses do not exhibit equal and opposite velocities. However, their initial approach velocity is essentially constant until they collapse at time $t=44\,000$ sec. A vertical arrow of length $7.5d$ has again been included as a length reference. The time origin of the graphs in Fig. 13 occurs at time $t=28\,250$ sec in this graph.

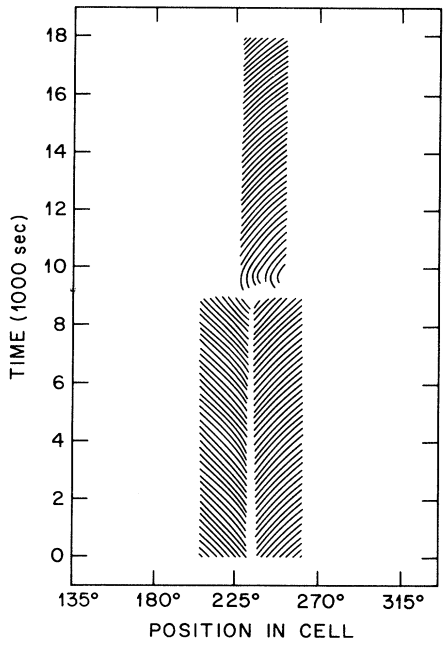

FIG. 15. Phase plot of the destruction of a state of two motionless, backward-facing pulses. Initially, the pulses coexisted at constant separation for many hours, at $v_{dr}=-0.0062\pm0.0005$ ($\bar{\epsilon}=-0.0123$). This caused the two pulses to move slowly together and to collapse at $t=9000$ sec, leading to the creation of a new pulse as in Fig. 13. Despite the extremely slow approach, the collapse of the double-pulse state was again essentially instantaneous.

transients typically last between 1 and 2×10^4 sec and necessitate extremely slow experimental measurements. The next increase in drift velocity in Fig. 17, to $+0.0010\pm0.0003$ [arrow (b)], caused a further increase in pulse separation. Now, however, the separation settled not to a constant value but to a constant, slightly positive separation velocity of magnitude 0.0002 (measured from times 4.3 to 5.8×10^4 sec in Fig. 17; the corresponding data point in Fig. 16 was also based on this time period). Because the pulses were moving slowly apart during this period, it cannot be claimed that a stable bound state had been formed. However, the velocity with which the pulses were separating during this period was extraordinarily small and was in fact significantly smaller than the velocity each pulse would have had if the other had been absent. Thus I conclude that the pulses were attracting one another. This was also the case following the next increase in the drift velocity, to 0.0022 ± 0.0004 at arrow (c). The subsequent separation velocity first assumed the value 0.0010 and then dropped to 0.0007. Both of these values are again significantly smaller than the drift velocity of an isolated pulse. Only after the last increase to $v_{dr}=0.0028\pm0.0004$ at arrow (d) did the pulse separation velocity increase to a value consistent with v_{dr}, indicating that neither pulse was slowing the drift of the other.

On the basis of the slowly increasing pulse separation seen at positive drift velocity in Fig. 17, it might be argued that the smooth curve in Fig. 16 has been drawn incorrectly, with its divergence at too positive a value of v_{dr}. Thus, because of the increasing pulse separation seen between arrows (c) and (d) in Fig. 17, one might insist that the corresponding data point in Fig. 16 should really represent a divergence in pulse separation at $v_{dr}=0.0022$. However, such an argument would be much weaker for the data point at $v_{dr}=0.0010$ and absolutely contradictory to the data at $v_{dr}=-0.0002$. Thus it appears that the curve in Fig. 16 really does cross the $v_{dr}=0$ axis with finite slope and diverges only at a truly positive value of

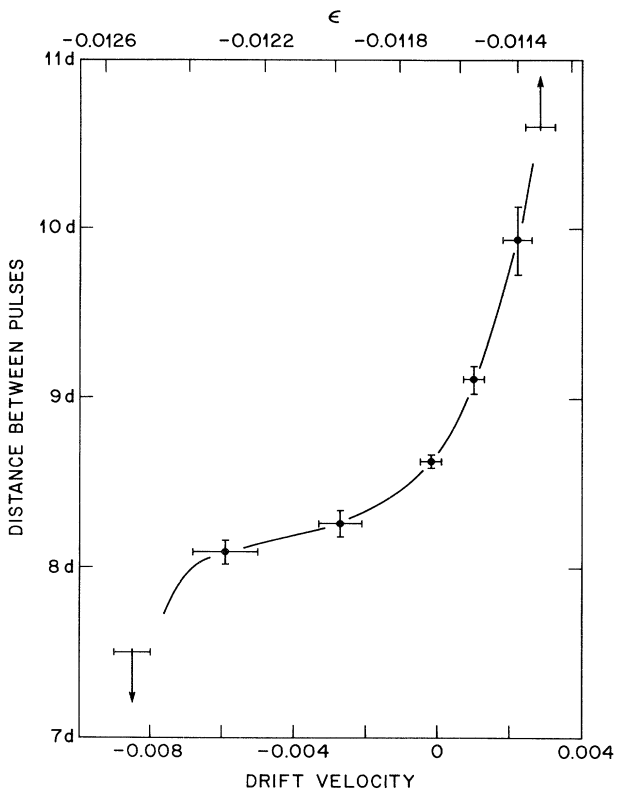

FIG. 16. The distance between the centroids of two backward-facing pulses is plotted as a function of drift velocity. As in Fig. 12, the scale on the top horizontal axis of the graph gives the value of ϵ corresponding to the drift velocity on the bottom horizontal axis. The arrow at $v_{dr}=-0.0085\pm0.0005$ represents the interaction in Fig. 15. As explained in Fig. 17, each of the two data points for $v_{dr}>0$ represents an unequilibrated state of two pulses which are drifting apart at a velocity that is less than that represented by the abscissa. The arrow at $v_{dr}=0.0028\pm0.0004$ represents a state in which the two pulses are drifting apart at the same velocity each would have if alone and are thus to be considered as noninteracting. The curve is a guide to the eye.

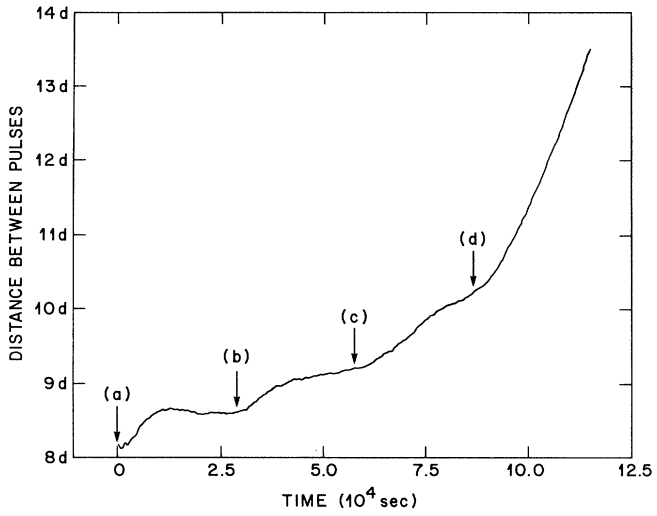

FIG. 17. The distance between the centroids of the two pulses represented in Fig. 16 is plotted as a function of time as the drift velocity is increased in steps from a slightly negative to a positive value. At time (a), v_{dr} is increased from -0.0027 ± 0.0006 to -0.0002 ± 0.0003. After a transient lasting about 2×10^4 sec, the pulse separation settles to a constant value of $8.62d\pm0.03d$. At time (b), v_{dr} is further increased to $+0.0010\pm0.0003$. After another transient, the pulses are seen to separate at an average velocity of 0.0002. The fact that this separation velocity is smaller than the drift velocity each pulse would have in the absence of the other suggests that the pulses are experiencing a mutual attraction, even though they no longer exhibit a strictly constant separation. At time (c) v_{dr} is increased to 0.0022 ± 0.0004. In response, the pulse separation velocity increases to 0.0010 and then drops to 0.0007; both values are still lower than the drift velocity of an isolated pulse. Finally, at time (d), v_{dr} is increased to 0.0028 ± 0.0004. The final separation velocity is the same (0.0031), suggesting that the pulses are no longer interacting.

v_{dr}, in contrast with the divergence at $v_{dr}=0$ observed in Fig. 12. There does indeed appear to be a bound double-pulse state in this experiment. However, it must be appreciated that the binding which holds the pulses together is extremely weak. Changing v_{dr} from 0.0010 to 0.0022 is accomplished by increasing ϵ by only 1.5×10^{-4}. The force of attraction between the two pulses barely exceeds the limit of detectability.

VI. DISCUSSION

This paper has described experiments which probe two aspects of pulses of traveling-wave convection: their interactions with localized features in the Rayleigh number and their behavior during binary collisions. Both of these series of experiments have been made possible by the sensitivity of the pulse drift velocity to the local Rayleigh number. Because of this behavior, the spatial profile of the stress parameter can be measured and corrected with extreme precision. With this technique, I have been able to fabricate a system which is uniform to parts in 10^5 in time and to parts in 10^4 in space. At present, the stability of the spatial uniformity appears to be limited by thermal drifts in the components in the trim-heating circuit. Modifications may allow further improvement.

Experiments on the interaction of drifting pulses with spatial variations in $\epsilon(x)$ have yielded poorly reproducible results for the interaction kernel. Part of the reason for this may be that the assumption that this interaction can be characterized by a simple convolution of the stress-parameter profile with a kernel of fixed shape is a poor one. Since the pulse changes shape as it drifts through regions of differing ϵ, the kernel which represents its behavior probably changes. It may also be simply unreasonable to try to represent the behavior of a nonlinear structure in this inherently linear manner. Nonetheless, these experiments appear to reveal a strong sensitivity of the pulse to the stress parameter far ahead of its own center of mass. This is an observation which might be easily reproduced in numerical calculations based on model equations.

The second subject of this paper has been collisions between pairs of traveling-wave pulses. These collisions are destructive if the approach velocity is too high. In the case of forward-facing pulses which collide at positive approach velocity, this interaction takes the form of one pulse gradually decaying in favor of the other. In the opposite case, two adjacent backward-facing pulses disappear abruptly and simultaneously, and a new pulse appears in their place after a short delay. In both cases, however, a double-pulse state can be created and maintained indefinitely by bringing two pulses together at extremely small velocity. Once formed, both forward-facing and backward-facing double-pulse states exist over a narrow range of Rayleigh number, and the typical pulse spacing is about $8d$—somewhat less than twice the pulse width—in both cases. The monotonic dependence of pulse separation on Rayleigh number (or, rather, on the bare drift velocity corresponding to the Rayleigh number) suggests that two adjacent forward-facing pulses do not form a true bound state. Rather, the state appears to be stable only because each pulse is drifting against a barrier presented by the other. The same situation seems to obtain in the case of adjacent backward-facing pulses, with the intriguing difference that, over a very narrow range of Rayleigh numbers at which the pulses slowly drift apart, they appear to attract each other weakly.

Interactions between pairs of TW pulses have been reported in two previous publications [6,7]. In both of these reports, the experimental control had not yet evolved to the level required to prevent destructive interactions. In Ref. [6], we suggested that the fate of a pair of adjacent pulses depends primarily on the perturbation each causes in the phase structure of the other. Phase perturbations at the trailing edge of a pulse seemed to be especially dangerous, because these are advected into the main body of the pulse and destabilize it by distorting its phase structure. Thus, in an adjacent pair of copropagating pulses, the leading pulse was seen to be rapidly destabilized, while forward-facing pulse pairs, in which there is no source of phase perturbations at the trailing edge of either pulse, seemed to be much more stable. From this point of view, one would predict that backward-facing pulse pairs ought to be less stable than forward-facing pairs, and this is indeed consistent with the observations presented in this paper. Forward-facing pulse pairs can be maintained over a range of drift velocity that is almost twice as wide as that over which backward-facing pulses persist—compare Figs. 12 and 16.

Barten, Lücke, and Kamps [17] have recently published the results of numerical integrations of the full Navier-Stokes equations which govern convection in binary fluids. For conditions near to those of the present experiment, they have been able to obtain a stable, pulse-shaped solution which appears to account very well for the properties of experimentally-observed pulses [7]. These calculations also reproduce quite well the properties of the confined states of arbitrary length seen at more negative values of the separation ratio [22]. One of the most interesting phenomena that has been revealed by this theoretical work is that nonlinear traveling-wave convection is accompanied by a large-scale lateral concentration flow. In the upper half of the fluid layer, the convection drives a flux of solute in the direction parallel to the roll propagation. A balancing flux is driven in the opposite direction in the lower-half of the fluid layer, so that there is no net transport of solute, in agreement with recent experiments [23]. In an extended state of traveling-wave convection in an infinite system, the large-scale concentration flow has no obvious physical consequences. However, the effect of this flow on a confined state such as a pulse is profound. In the quiescent region just ahead of the leading edge of a pulse, the advected concentration fluxes enhance the preexisting vertical concentration gradient caused by the Soret effect. This decreases the buoyant force in this region, stabilizing it against convection and causing the front between the convecting and nonconvecting regions to propagate into the latter region much more slowly than the speed of the rolls behind the front. This process has recently been visualized directly [24]. Conversely, the quiescent region

just behind the trailing edge of the pulse is destabilized against convection, so that this region is "filled in" with rolls as they pass into the body of the pulse. These effects are responsible for the slow propagation and fixed shape of traveling-wave pulses.

The observation that pairs of forward-facing pulses behave as if they repel one another is not surprising in light of these theoretical results. If a large-scale concentration circulation acts to stabilize the region ahead of an isolated pulse, this effect could only be enhanced in the region between two forward-facing pulses. However, the observation of persistent backward-facing pulse pairs is somewhat of a surprise in this context, because one would expect that the region between two such pulses would be even less stable to convection than it would be if only one pulse were present. In practice, backward-facing pulse pairs are observed to annihilate at a slightly larger pulse spacing than forward-facing pulse pairs ($\sim 8.0d$ vs $\sim 7.6d$, from Figs. 12 and 16), and this is what one would expect in light of the theory. However, the difference between these two numbers is very slight. The observation of a weak attraction between pairs of very slowly moving backward-facing pulses would also appear to run counter to intuition based on the theoretical results. Clearly, these experimental results pose interesting problems for further theoretical work based on numerical integrations of the Navier-Stokes equations.

Model equations such as the CGLE offer the possibility of explaining the dynamical behavior of pulses using simpler numerical tools than those required for the study of the full Navier-Stokes equations. In this approach, the fast variations associated with the propagation of the underlying TW are averaged out, yielding a theory for the amplitude of convection [12]. Thus the evolution of the fast phase structure seen in some of these experiments cannot be described by a model of this type. Nonetheless, such models still have a term containing the group velocity, which is related to the TW phase velocity. In the case of counterpropagating pulses, there is no frame of reference in which this term vanishes, and the direction of propagation of the underlying TW retains its significance.

Two approaches to understanding pulse interactions on the basis of model equations have recently been taken. Malomed [25] has studied the interactions between overlapping pulses in a comoving frame using a perturbation analysis of coupled subcritical CGLE's. In his theory, nearby pulses are found to experience a weak attractive potential in the limit of vanishing nonlinear dispersion. In the opposite, nonlinear-Schrödinger-equation limit, true solitons which bind weakly are observed as well. However, this theory is not directly applicable to case of counterpropagating pulses addressed in these experiments. Indeed, controlled experiments on collisions between copropagating pulses would be quite difficult, since such pulses could be made to approach one another only by applying a precisely controlled gradient in $\epsilon(x)$. Deissler and Brand [18] have studied collisions between truly counterpropagating pulses in numerical integrations of coupled subcritical CGLE's which retain the group-velocity terms. The inclusion of nonlinear gradient terms introduces parameters which change the shape and propagation velocity of the pulses. Comparison of these changes with the measurements presented in Ref. [7] may allow the definition of a theoretical parameter which has the same effect on pulse properties as the Rayleigh number does in experiment. In the experimentally relevant case of stabilizing cross-coupling, binary collisions between pulses have been observed to have only two outcomes in these calculations: both pulses either die during the collision or survive it, passing through one another and propagating as before. Neither of these cases matches the experimental observations. However, these computations explored only a rather narrow region of a wide, multidimensional parameter space. It may be that, if the numerical parameters are adjusted so that the computed static properties of isolated pulses explicitly match the experiments in Ref. [7], then their collisions will better duplicate the results presented here. The correct description of the shape and drift of isolated pulses as well as the nature of various types of pulse collisions would constitute a major success for a phenomenological model of traveling-wave pulses.

ACKNOWLEDGMENTS

I am pleased to acknowledge discussions with P. C. Hohenberg, B. L. Winkler, H. R. Brand, B. I. Shraiman, and B. A. Malomed.

[1] R. W. Walden, P. Kolodner, A. Passner, and C. M. Surko, Phys. Lett. **55**, 496 (1985).

[2] E. Moses, J. Fineberg, and V. Steinberg, Phys. Rev. A **35**, 2757 (1987); R. Heinrichs, G. Ahlers, and D. S. Cannell, *ibid.* **35**, 2761 (1987).

[3] P. Kolodner, D. Bensimon, and C. M. Surko, Phys. Rev. Lett. **60**, 1723 (1988); D. Bensimon, P. Kolodner, C. M. Surko, H. Williams, and V. Croquette, J. Fluid Mech. **217**, 441 (1990).

[4] J. J. Niemela, G. Ahlers, and D. S. Cannell, Phys. Rev. Lett. **64**, 1365 (1990).

[5] K. E. Anderson and R. P. Behringer, Phys. Lett. A **145**, 323 (1990).

[6] P. Kolodner and J. A. Glazier, Phys. Rev. A **42**, 7504 (1990); J. A. Glazier and P. Kolodner, *ibid.* **43**, 4269 (1991).

[7] P. Kolodner, Phys. Rev. Lett. **66**, 1165 (1991); preceding paper, Phys. Rev. A **44**, 6448 (1991).

[8] V. Steinberg, E. Moses, and J. Fineberg, Nucl. Phys. B (Proc. Suppl.) **2**, 109 (1987).

[9] P. Kolodner and C. M. Surko, Phys. Rev. Lett. **61**, 842 (1988); J. Fineberg, E. Moses, and V. Steinberg, *ibid.* **61**, 838 (1988); P. Kolodner, C. M. Surko, and H. Williams, Physica D **37**, 319 (1989); V. Steinberg, J. Fienberg, E. Moses, and I. Rehberg, *ibid.* **37**, 359 (1989).

[10] O. Thual and S. Fauve, J. Phys. (Paris) **49**, 1829 (1988); O. Thual and S. Fauve, Phys. Rev. Lett. **64**, 282 (1990).

[11] W. van Saarloos and P. C. Hohenberg, Phys. Rev. Lett. **64**, 749 (1990), and (unpublished).

[12] A. C. Newell, in *Nonlinear Wave Motion,* edited by A. C.

Newell, Lectures in Applied Mathematics Vol. 15 (AMS, Providence, 1974), p. 157.

[13] S. J. Linz and M. Lücke, Phys. Rev. A **35**, 3997 (1987); B. J. A. Zielinska and H. R. Brand, *ibid.* **35**, 4349 (1987); E. Knobloch and D. R. Moore, *ibid.* **37**, 860 (1988); M. C. Cross and K. Kim, *ibid.* **37**, 3909 (1988).

[14] W. Schöpf and W. Zimmerman, Europhys. Lett. **8**, 41 (1989); W. Schöpf and L. Kramer, Phys. Rev. Lett. **66**, 2316 (1991).

[15] C. M. Surko and P. Kolodner, Phys. Rev. Lett. **58**, 2055 (1987); P. Kolodner, C. M. Surko, H. L. Williams, and A. Passner, in *Propagation in Systems Far from Equilibrium,* edited by J. E. Wesfreid *et al.* (Springer-Verlag, Berlin, 1988), p. 282; P. Kolodner, C. M. Surko, and M. C. Cross (unpublished).

[16] P. Kolodner, J. A. Glazier, and H. Williams, Phys. Rev. Lett. **65**, 1579 (1990); J. A. Glazier, P. Kolodner, and H. Williams, J. Stat. Phys. **64**, 945 (1991).

[17] W. Barten, M. Lücke, and M. Kamps, Phys. Rev. Lett. **66**, 2621 (1991).

[18] H. R. Brand and R. J. Deissler, Phys. Rev. Lett. **63**, 2801 (1989); R. J. Deissler and H. L. Brand, Phys. Lett. A **146**, 252 (1990).

[19] P. Kolodner and H. Williams, in *Proceedings of the NATO Advanced Research Workshop on Nonlinear Evolution of Spatio-temporal Structures in Dissipative Continuous Systems,* Vol. 225 of *NATO Advanced Study Institute Series B2,* edited by F. H. Busse and L. Kramer (Plenum, New York, 1990), p. 73.

[20] P. Kolodner, H. Williams, and C. Moe, J. Chem. Phys. **88**, 6512 (1988).

[21] It should be noted that the experiments reported in this paper were performed during two separate time periods and used two different fluids which, while nominally identical, in fact exhibited slightly different dependences of pulse drift velocity on ϵ. Thus the curve in Fig. 1 does not exactly match that in Fig. 15 of Ref. [7]. This earlier curve was used to calibrate the vertical axes in Figs. 2, 3, and 6, while Fig. 1 pertains to the rest of the data presented in this paper. It should also be noted that the velocities quoted in describing the pulse-collision results in Sec. V were separately measured in repeated calibration runs interspersed with collision experiments, in order to minimize velocity-calibration drifts.

[22] C. M. Surko, D. R. Ohlsen, S. Y. Yamamoto, and P. Kolodner, Phys. Rev. A **43**, 7101 (1991).

[23] P. Kolodner, Phys. Rev. A **42**, 7204 (1990).

[24] B. L. Winkler and P. Kolodner (unpublished).

[25] B. A. Malomed, this issue, Phys. Rev. A **44**, 6954 (1991).